Anomalous Hall Effect and Quantum Criticality in Geometrically Frustrated Heavy Fermion Metals

Wenxin Ding,[1,2,*] Sarah Grefe,[3,2,*] Silke Paschen,[4] and Qimiao Si[2]
[1]School of Physics and Optoelectronics Engineering, Anhui University, Hefei, Anhui Province 230601, China
[2]Department of Physics & Astronomy, Rice University, Houston, Texas 77005, USA
[3]Department of Physics & Astronomy, California State University, Long Beach, California 90840, USA
[4]Institute of Solid State Physics, Vienna University of Technology, Wiedner Hauptstraße 8-10, 1040 Vienna, Austria

(Received 9 April 2023; revised 21 April 2024; accepted 9 July 2024; published 6 September 2024)

Studies on the heavy-fermion pyrochlore iridate ($Pr_2Ir_2O_7$) point to the role of time-reversal-symmetry breaking in geometrically frustrated Kondo lattices. Here, we address the effect of Kondo coupling and chiral spin liquids in a J_1-J_2 model on a square lattice and a model on a kagome lattice via a large-N method, based on a fermionic representation of the spin operators, and consider a new mechanism for anomalous Hall effect for the chiral phases. We calculate the anomalous Hall response for the chiral states of both the Kondo destroyed and Kondo screened phases. Across the quantum critical point, the anomalous Hall coefficient jumps when a sudden reconstruction of Fermi surfaces occurs. We discuss the implications of our results for the heavy-fermion pyrochlore iridate and propose an interface structure based on Kondo insulators to explore such effects further.

DOI: 10.1103/PhysRevLett.133.106504

Heavy-fermion metals are prototypical systems to study quantum criticality [1–3]. The simplest model to describe these systems is a Kondo lattice, which comprises a lattice of local moments and a band of conduction electrons. The local moments are coupled to each other by the Ruderman-Kittel-Kasuya-Yosida interaction and are simultaneously connected to a band of conduction electrons through an antiferromagnetic (AFM) Kondo exchange interaction (J_K). In recent years, it has been realized that the effect of geometrical frustration is a potentially fruitful but little-explored frontier. From a theoretical perspective, geometrical frustration enhances G, the degree of quantum fluctuations in the magnetism of the local-moment component, and a J_K-G phase diagram at zero temperature has been advanced [4,5]. Figure 1(a) illustrates the proposed global phase diagram [4], which applies the notion of Kondo destruction [6] to the parameter space that incorporates the frustration and related quantum fluctuation effects. From a materials perspective, there is a growing effort in studying frustrated Kondo-lattice compounds [7–14].

The pyrochlore heavy-fermion system $Pr_2Ir_2O_7$ is one such example. Both the measured magnetic susceptibility and specific heat [11] suggest the presence of Kondo coupling between the Ir d electrons and the local f moments of Pr. No magnetic order is found down to very low temperatures, suggesting that the f moments of Pr develop a quantum spin liquid (QSL) ground state [11]. In addition, experiments found a sizable anomalous Hall effect (AHE) based on extrapolating the magnetic field applied along the [111] direction to zero [15,16], revealing a spontaneous time-reversal-symmetry-breaking (TRSB) state.

This system is of considerable theoretical interest [17–23]. With a few exceptions [24], the role of the Kondo effect has not been discussed in this context, and neither has its relationship with the observed quantum criticality. Yet, the observation of a large entropy and a divergent Grüneissen ratio [25] clearly points to the importance of the Kondo coupling and the role of a proximate heavy-fermion quantum critical point (QCP). In the case of AFM heavy-fermion systems, the normal Hall effect has been successfully used to probe the evolution of the Fermi surface across the QCP and, thereby, the nature of quantum criticality [3,14,26]. Given that the AHE is also intrinsically a Fermi surface property (other than contributions from fully occupied bands) [27], we are motivated to address whether it can serve as a diagnostic tool for the QCP in the present setting. In addition to elucidating the AHE, studying this issue promises to bring about the much-needed new understanding of quantum phases and their transitions in geometrically frustrated heavy-fermion metals [14]. Given the complexity of the three-dimensional pyrochlore lattice, we will gain insights from related but simpler models.

In this Letter, we study both the frustrated J_1-J_2 quantum Heisenberg model on a square lattice and the J_1 only model on the kagome lattice with a Kondo coupling to conduction electrons. For the square lattice, we consider the regime of strong frustration where a chiral spin liquid (CSL) phase [28] becomes energetically competitive in a large-N limit

*These authors contributed equally to this work.

(based on a Schwinger fermion representation of the spin operators; see below). The kagome lattice, representing a layer perpendicular to the [111] direction of the pyrochlore lattice, is a two-dimensional network of corner-sharing triangles [Fig. 1(d)] with a strong geometrical frustration. A CSL phase is found in a spin-$\frac{1}{2}$ model on the kagome lattice [29]. Using the large-N limit [30], we will also study the CSL physics on this lattice. We develop the method to calculate the AHE in both a Kondo-destroyed (P_S) and a Kondo-screened (P_L) paramagnetic phase. We show that each phase may have a sizable AHE. Moreover, across a QCP, the AHE jumps when the Fermi surface suddenly reconstructs.

Frustrated Kondo-lattice models—We study the following Hamiltonian:

$$H = H_f + H_{d,0} + H_K. \tag{1}$$

Here, H_f describes a Heisenberg model. For the square lattice case, H_f includes both J_1 and J_2 couplings between the nearest neighbors (nn, $\langle\rangle$) and next-nearest neighbors (nnn, $\langle\langle\rangle\rangle$). We focus on the maximally frustrated case of $J_2/J_1 = 1/2$. For the kagome case, the lattice is geometrically frustrated and it suffices for H_f to only contain the nn term. For both models with H_f alone, CSL states appear in the large-N limit [28,31].

The local moments are coupled to a band of conduction electrons, described by $H_{d,0} = -\sum_{ij,\alpha}(t_{ij} d^\dagger_{i\alpha} d_{j\alpha} + \text{H.c.})$, through an AFM Kondo interaction J_K, specified by $H_K = J_K \sum_i \boldsymbol{s}_i \cdot \boldsymbol{S}_i$. Here, $\boldsymbol{s}_i = \sum_{\alpha,\beta} \frac{1}{2} d^\dagger_{i\alpha} \boldsymbol{\sigma}_{\alpha\beta} d_{i\beta}$ is the spin of the conduction electrons, with $\boldsymbol{\sigma}$ describing the Pauli matrices. We take $t_{\langle ij\rangle} = t = 1$ as the energy unit.

We use the Schwinger fermion representation for the f-moments $\boldsymbol{S}_i = \sum_{\alpha,\beta} \frac{1}{2} f^\dagger_{i\alpha} \boldsymbol{\sigma}_{\alpha\beta} f_{i\beta}$, with the constraint $\sum_\alpha f^\dagger_{i\alpha} f_{i\alpha} = 1$, so that $H_f = \sum_{\alpha,\beta,ij} (J_{ij}/2) f^\dagger_{i\alpha} f_{i\beta} f^\dagger_{j\beta} f_{j\alpha} - (J_{ij}/4) n_{i\alpha} n_{j\beta}$. In the large-$N$ approach [31], the spin index $\alpha = 1, 2, \ldots, N$, and the constraint is enforced by a Lagrangian multiplier λ_i. The Heisenberg and Kondo terms are decoupled by a Hubbard-Stratonovich (HS) transformation. The large-N limit leads to

$$H_{\text{eff}} = H_{\text{QSL}} + H_{d,0} + H_{K,\text{eff}} + E_c, \tag{2}$$

with $H_{\text{QSL}} = -\sum_{ij,\alpha}(J_{ij}/2)(\chi_{ji} f^\dagger_{i\alpha} f_{j\alpha} + \text{H.c.}) - \sum_{i,\alpha} \lambda_i \times (f^\dagger_{i\alpha} f_{i\alpha} - 1/2)$, $H_{K,\text{eff}} = -\sum_{i,\alpha}(J_K/2)(\pi_i d^\dagger_{i\alpha} f_{i\alpha} + \text{H.c.})$, and $E_c = \sum_{ij} N J_{ij} |\chi_{ij}|^2/2 + \sum_i N J_K |\pi_i|^2/4$. The HS fields are defined as $\chi_{ij} = \sum_\alpha \langle f^\dagger_{i\alpha} f_{j\alpha}\rangle$ and $\pi_i = \sum_\alpha \langle f^\dagger_{i\alpha} d_{i\alpha}\rangle$. Both can be decomposed into amplitudes and phases: $\chi_{ij} = \rho_{ij} e^{iA_{ij}}$, $\pi_i = \rho_{K,i} e^{iA_{K,i}}$. The Kondo parameter π_i can be taken to be real, with its phase absorbed into the field λ_i, i.e. $\pi_i \to \rho_{K,i}$.

By minimizing the total energy of H_{eff} in Eq. (2), we obtain the phase diagrams containing the chiral states, in which J_K tunes the system from the P_S to P_L phases (see Supplemental Material [32]). Across a second-order Kondo-destroyed $P_{S,\text{chiral}}$ to $P_{L,\text{chiral}}$ quantum phase transition, Fig. 1(b), we consider a power-law form for the Kondo hybridization amplitude:

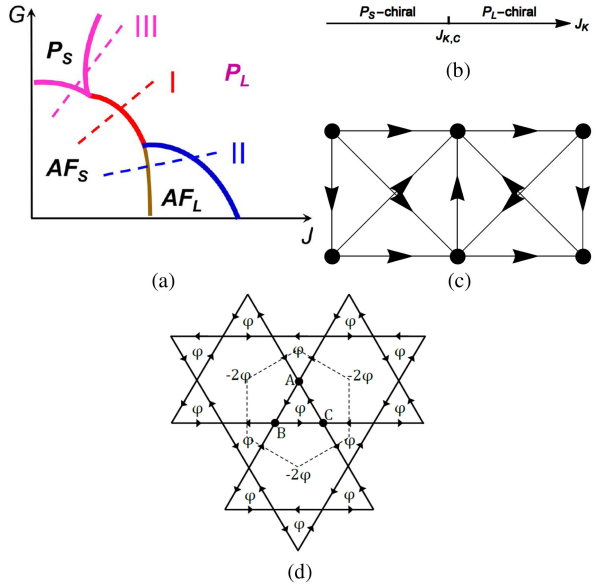

FIG. 1. (a) The global phase diagram of Kondo lattice systems [4]; (b) in the highly frustrated regime (large, fixed G), J_K tunes through a Kondo-destruction QCP (at $J_{K,c}$) from a Kondo-destroyed chiral spin liquid ($P_{S,\text{chiral}}$) to a Kondo-screened phase ($P_{L,\text{chiral}}$). The χ fields of the square lattice are shown in the π-flux state (without the diagonal bonds) and the CSL state (c), and in the CSL state on the kagome lattice (d). The arrows denote the sign of gauge field A_{ij}, and ϕ is the flux through a triangle.

$$\rho_K(J_K) = \rho_r \left(\frac{J_K - J_{K,c}}{J_K}\right)^{1/2}, \tag{3}$$

for $J_K > J_{K,c}$ and $\rho_K = 0$, for $J_K < J_{K,c}$. We take $J_{K,c}$ as the value where the $P_{L,\text{chiral}}$ state becomes energetically competitive and ρ_r to be the saturation value of ρ_K; both values are adopted from the self-consistent calculation for a given set of (n_d, J_1) [32].

Mechanism of the AHE: the Kondo destroyed P_S phase—In the Kondo-destroyed P_S phase, the static hybridization amplitude vanishes, $\langle \rho_{K,i} \rangle = 0$. However, we show that there are TRSB terms in the effective interactions among the conduction electrons, which are mediated by the spinons via Kondo couplings. Such terms yield a zero-field AHE.

We will single out the TRSB terms. The TRSB order parameter of the CSL is the spin chirality,

$$\hat{E}_{ijk} = \boldsymbol{S}_i \cdot (\boldsymbol{S}_j \times \boldsymbol{S}_k), \tag{4}$$

where the indices $\{i, j, k\}$ mark the three sites of an elementary triangle of the lattice. In the CSL state,

$E_{ijk} = \langle \hat{E}_{ijk} \rangle = 2i(P_{ijk} - P_{ikj})$, where $P_{ijk} = \chi_{ij}\chi_{jk}\chi_{ki}$. On symmetry grounds, we expect E_{ijk} to be coupled to the composite chiral operator of the conduction electrons, $\boldsymbol{s}_i \cdot (\boldsymbol{s}_j \times \boldsymbol{s}_k)$. With this guidance, we obtain the coupling from integrating out the f fermions and expanding in powers of J_K; this can be represented by triangular diagrams (Supplemental Material [32]), similar to what is used in deriving a chiral current. We find

$$H_{\text{chiral}} = \sum \frac{J_K^3}{3!} \underbrace{(\boldsymbol{s}_i \cdot \boldsymbol{S}_i)(\boldsymbol{s}_j \cdot \boldsymbol{S}_j)(\boldsymbol{s}_k \cdot \boldsymbol{S}_k)}_{\Delta\text{-loop contraction}} = \frac{J_K^3}{2 \times 3!} E_{ijk} \boldsymbol{s}_i \cdot (\boldsymbol{s}_j \times \boldsymbol{s}_k). \tag{5}$$

In the kagome case, the hexagons can also possess nontrivial fluxes. However, we can restrict the effective TRSB coupling for the conduction electrons to the lowest order in J_K, which corresponds to considering only the fluxes of the triangles.

The chiral interactions in H_{chiral} have a six-fermion form. We can decouple it by introducing a novel HS transformation that involves triangular diagrams described in Supplemental Material [32]. We end up with an effective bilinear theory:

$$H_d = H_{d,0} + H_{d,1}, \tag{6}$$

with

$$H_{d,1} = \sum_{ij} (g\phi_j^* \phi_i d_i^\dagger d_j + \phi_i^* G_{\phi,ij}^{-1} \phi_j + \text{H.c.}). \tag{7}$$

Hence, the ϕ fields are constrained by the condition that, if they are integrated out, we obtain the same chiral interaction terms at $\mathcal{O}(g^3)$ by computing the same triangle diagrams. We then replace $\phi_j^* \phi_i$ by its expectation value $G_{\phi,ij}$ and arrive at

$$H_{d,1} \to \sum_{ij} (g G_{\phi,ij} d_i^\dagger d_j + \text{H.c.}). \tag{8}$$

It turns out that $G_{\phi,ij} = e^{-iA_{ij}}$, and g can be identified as $g = J_K(|E_{ijk}|/2)^{1/3}$. Because the bosonic Gaussian integral has a minus sign relative to its fermionic counterpart, $G_{\phi,ij}$ carries the opposite flux pattern to produce the same H_{chiral} when we integrate out the ϕ fields. Physically, the flux (or chirality) pattern has the opposite sign to that of the CSL state, so that the antiferromagnetic Kondo coupling will lower the ground state energy. This effective Hamiltonian is adequate for qualitatively describing the AHE physics of our original Hamiltonian. Other nonchiral effective interactions would only renormalize the Fermi liquid parameters of the d electrons for the P_S phase. We can then use the Streda formula [38,39] to compute the AHE coefficient σ_{xy}: The involved quantities are the current operator of the conduction electrons $v_a(\mathbf{k}) = \partial_a H_d(\mathbf{k})$, the Berry curvature $\mathcal{F}_n^{xy}(\mathbf{k})$, and the Fermi function $f[\epsilon_n(\mathbf{k})]$ (Supplemental Material [32]).

Mechanism of the AHE: the Kondo screened P_L phase—In the P_L phase, the Kondo order parameter $\rho_{K,i}$ acquires a nonzero expectation value $\rho_K = \langle \rho_{K,i} \rangle$. There should still be an incoherent piece of the slave boson fields: $\rho_{K,i} = \rho_K + \pi_i'$. Moreover, we focus on the case where the chiral order survives in the P_L phase. By considering the same triangular diagrams now mediated by the incoherent part π_i', the fluctuations of the Kondo order parameter still mediate chiral interactions similarly as in the P_S phase, but with a reduced weight. However, there is no spectral sum rule for the π_i's to obtain this reduced weight readily. In Supplemental Material [32], we use a slave rotor approach for the periodic Anderson model to determine this factor. The effective Hamiltonian of the d electrons becomes

$$H_d = H_{d,0} + [1 - (4J_K/U)\rho_K^2] H_{d,1}, \tag{9}$$

where U is the onsite Hubbard repulsion. We fix $U = 2W$, i.e., twice the d electron's bandwidth throughout the calculations. Keeping only the ρ_K part of H_K leads to the following effective Hamiltonian:

$$H_{P_L} = \Psi^\dagger \begin{pmatrix} H_{\text{CSL}} & -J_K \rho_K \mathcal{I} \\ -J_K \rho_K \mathcal{I} & H_d \end{pmatrix} \Psi, \tag{10}$$

where $\mathcal{I}$ is an identity matrix, and $\Psi^\dagger = (f^\dagger, d^\dagger)$. We have dropped the spin index, as there are no longer spin-flip terms. The Hamiltonian H_{P_L} is smoothly connected with H_d at the QCP. We then compute σ_{xy} from the Streda formula Eq. (S-22) [32] noting that the current operators remain the same, i.e., $v_a(\mathbf{k}) = \partial_a H_d(\mathbf{k})$.

AHE and its evolution across the Kondo-destruction QCP—For the square lattice, we focus on the π flux and the CSL states which are known to be closely competing in the pure J_1-J_2 Heisenberg models. In the large-N calculation based on Eq. (10), we find that both states can be stabilized in the presence of Kondo screening. The P_L-CSL state emerges as the ground state first, but the P_L-π–flux state eventually takes over at larger J_K/J_1 [see Fig. (S5) and related Supplemental Material for details [32]].

For the π-flux phase, $H_{\text{QSL}} = H_{\pi\,\text{flux}}$ is given by $A_{\boldsymbol{r}_i,\boldsymbol{r}_i+\hat{x}} = \pi/2$, $A_{\boldsymbol{r}_i,\boldsymbol{r}_i+\hat{y}} = -(-1)^{x_i}\pi/2$, $\rho_{\boldsymbol{r}_i,\boldsymbol{r}_i+\hat{x}+\hat{y}} = 0$, where $\boldsymbol{r}_i = (x_i, y_i)$, $\hat{x}$ ($\hat{y}$) is the unit vector along the $x(y)$ axis. For the CSL Hamiltonian, $H_{\text{QSL}} = H_{CSL}$ is derived from $H_{\pi\,\text{flux}}$ with $\rho_{\boldsymbol{r}_i,\boldsymbol{r}_i+\hat{x}+\hat{y}} \neq 0$, $A_{\boldsymbol{r}_i,\boldsymbol{r}_i+\hat{x}+\hat{y}} = A_{\boldsymbol{r}_i+\hat{y},\boldsymbol{r}_i+\hat{x}} = (-1)^{x_i}\pi/2$, as illustrated in Fig. 1(c).

In the kagome lattice, any state with triangle flux $\phi \neq 0, \pi$ breaks time-reversal symmetry (TRS). Here, we choose

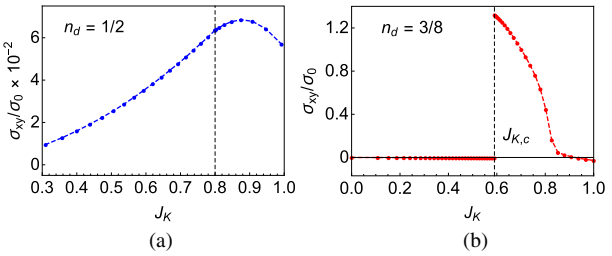

FIG. 2. Zero field anomalous Hall conductance (σ_{xy}), normalized by the quantum conductance $\sigma_0 = e^2/h$, for $J_1 = t = 1$, $J_2/J_1 = 1/2$, $n_d = 0.5$ on a square lattice (a) and for $J = t$, $n_d = 3/8$ on a kagome lattice (b).

$\phi = -(\pi/2)$ such that the hexagon flux of $-2\phi = \pi$ preserves TRS. The $[-(\pi/2), \pi]$ spinon flux state has three well-separated bands; the middle flat band is exactly at the Fermi energy, and the Chern numbers are $C_{\text{lower}} = -1$, $C_{\text{middle}} = 0$, $C_{\text{upper}} = +1$ [39]. These band structures can be considered the usual, no-flux kagome bands inverted by the fluxes. The phase structure of the corresponding χ_{ij} fields is plotted in Fig. 1(d).

The zero-field anomalous Hall conductivity σ_{xy} of the J_1-J_2-J_K model is shown in Fig. 2(a) for representative parameters $n_d = 0.5$, $J_1 = t$ and that of the kagome lattice model in Fig. 2(b) for $J = t$, $n_d = 3/8$. Across the QCP, σ_{xy} is found *continuous* for the square lattice, but *jumps discontinuously* for the kagome lattice. The amplitudes of σ_{xy} are similar in the P_S regimes, $\sim 10^{-2}\sigma_0$. But σ_{xy} is enhanced by 2 orders of magnitude in the P_L regime of the kagome case.

In order to understand the different behaviors, we show the Fermi surfaces (dashed lines) and the difference of band-summed Berry curvature $\Delta\Omega(\mathbf{k})$ (color map) between the P_S phase and the P_L phase right across the QCP in Figs. 3(a) for the square lattice and 3(b) for the kagome lattice [the actual $\Omega(\mathbf{k})$ is shown in Supplemental Material [32]]. Here, $\Delta\Omega(\mathbf{k}) = \Omega_{P_S}(\mathbf{k}) - \Omega_{P_L}(\mathbf{k})$ and

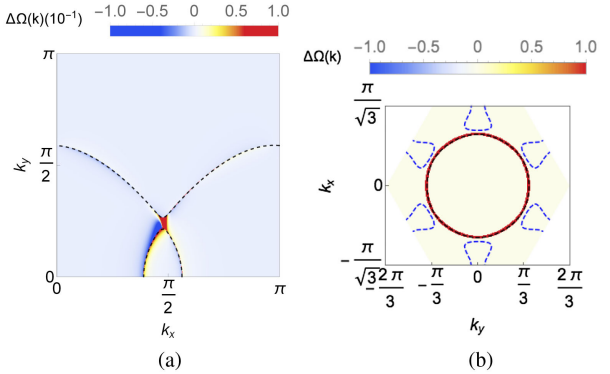

FIG. 3. Fermi surfaces (dashed curves) and the difference in the band-summed Berry curvature distribution $\Delta\Omega(\mathbf{k})$ between the P_S phase and the P_L phase (color map) of the square lattice model (a) and the kagome lattice model (b).

$\Omega(\mathbf{k}) = \sum_n \mathcal{F}_n^{xy}(\mathbf{k}) f[\epsilon_n(\mathbf{k})]$. We find the Fermi surfaces remain continuous for the square lattice model. Both Fermi surfaces of the P_S and P_L phases are the black dashed line. However, for the kagome case, the Fermi surfaces show a jump. The Fermi surface of the P_S phase is the black dashed circle in the middle of the BZ which overlaps with the red, singular part of $\Delta\Omega(\mathbf{k})$. Those of the P_L phase are the blue-dashed-line pockets at the edge of the BZ. These results reflect the number of sites per unit cell and the gapped-gapless nature of the spinon spectrum. However, $\Delta\Omega(\mathbf{k})$ is singular and concentrates near Fermi surfaces in both cases. This is because the onset of Kondo hybridization, which acts as a topological mass term in the large-N theory, in general singularly reconstructs the wave functions regardless of whether the Fermi surfaces jump or not.

To reconcile the notions of the singular wave function (or Berry curvature) with the continuous AHE, we note that σ_{xy} is intrinsically a Fermi surface property [27] (apart from the contributions of fully occupied bands). We can analytically show the following by computing the diagonal Berry's connection in the $\rho_K \to 0$ limit [32]. When the Fermi surfaces evolve continuously across the QCP, σ_{xy} must be continuous; here, the projected wave functions of the d-electron are continuous, and so are the Berry connections. By contrast, when the Fermi surface jumps, the projected wave functions completely reconstruct due to the existence of two noncommuting topological "masses": the Kondo screening and a nonzero jump of the spinon Lagrangian multiplier λ.

Discussion—Energetic considerations [40] show that the Kondo coupling favors gapless spin-liquid states over their gapped counterparts (Supplemental Material [32]); in the absence of a spinon gap, it is easier to form a Kondo singlet, which lowers the energy by an amount $\propto J_K$. For the pyrochlore lattice, the CSL state in the large-N limit is gapless [41], and is thus expected to have a similar sequence of quantum phase transitions involving the chiral state. The gapless nature raises the prospect of a sudden reconstruction of the Fermi surface across a Kondo-destruction QCP in the pyrochlore case and, by extension, a jump in the extrapolated zero-field AHE, especially for a magnetic field along the [111] direction.

We expect the jump of the zero field AHE, σ_{xy}, to be robust against weak disorder. The AHE effect considered here is intrinsic, i.e., determined by the quasiparticle band structure. Scattering from weak nonmagnetic impurities only yields a small (linear in disorder) correction [42]. Moreover, the Fermi-surface jump across a Kondo-destruction QCP has been evidenced to be robust against weak disorder [12,43]. Thus, our results can be tested in $Pr_2Ir_2O_7$, once a control parameter is identified to tune across the implicated zero-field QCP [25]. From Ref. [44], strain can potentially serve as such a tuning parameter.

We note that the anomalous Hall conductance from the mechanism advanced here is quite large. Experiments in

$Pr_2Ir_2O_7$ [16] find a large sheet σ_{xy} reaching about 0.7% of $\sigma_0 \equiv e^2/h$, a value which can readily arise in our mechanism [Fig. 2(a)].

We have emphasized the role of the Kondo effect and its critical destruction. Future work should incorporate *ab initio* features, not only on the directional dependence in the pyrochlore lattice but also the effect of the *ab initio* electronic band structure and the non-Kramers nature of the ground-state crystal-field level of the Pr ions [24,45]. Although Ref. [24] studied a realistic model, the mechanism of AHE in the Kondo destroyed phase is not captured, and $\sigma_{xy}^{\mathrm{AHE}}$ only starts to grow from zero at the QCP. The new mechanism we consider here provides a possible interpretation to the experimental observation that $\sigma_{xy}^{\mathrm{AHE}}$ is most singular at the QCP.

Furthermore, we have derived our conclusions in geometrically frustrated Kondo systems and demonstrated the robustness of our results by connecting them with the evolution of the Fermi surfaces. Thus, we expect our results to remain qualitatively valid in the more realistic settings. For $Pr_2Ir_2O_7$, this is so given the substantial evidence for the role of the Kondo coupling such as the large entropy observed in the pertinent low-temperature regime [25]. It may also be instructive to explore related effects in other f-electron systems with geometrical frustration, such as UCu_5 under ambient conditions [46] and when suitably tuned through a QCP. Recently, the proximity to the Kondo-destruction QCP we predict here for $Pr_2Ir_2O_7$ is confirmed experimentally [47]. In this STM measurement, regions of heavy Fermi liquid are interweaved with a nonmagnetic metallic phase with Kondo destruction, forming spatial nanoscale patterns consistent with being in proximity to a critical point.

While the current work emphasizes the link between AHE and the evolution of Fermi surfaces due to Kondo physics, other topology-related components, such as conduction band topology, k dependence of Kondo coupling, etc., are not taken into account. It is known that such components can lead to topological Kondo lattice models that realize such topological states as Weyl-Kondo semimetals [48–51]. In addition, d-electron-based systems on frustrated lattices, through the notion of compact molecular orbitals, can realize topological Kondo lattice models and the associated states [52–54]. For these states, the Berry-curvature-induced Hall effect is also an important characteristic; thus, we expect our work here will provide new insights into those systems.

We close by proposing an engineered Kondo-insulator interface as a model material for the frustrated Kondo lattice Hamiltonian. The motivation for the proposed setting comes from advances in the molecular beam epitaxy (MBE) of Kondo systems [55–57]. As a promising candidate material, we suggest the golden phase of SmS (g-SmS). In bulk samples, this phase is stable under pressures between about 0.65 GPa [58] and 2 GPa [59]. As MBE thin film, the phase might be stabilized by lattice mismatch with an appropriate substrate. g-SmS crystallizes in a face-centered-cubic (fcc) structure of rocksalt (NaCl) type. A lattice plane is shown in Fig. (S6). g-SmS shows characteristics of a Kondo insulating state in transport [59,60], thermodynamics [61], and point contact spectroscopy [60]. From thermal expansion and heat capacity measurements, the energy gap was estimated to be 90 K on the low-pressure side of the g-SmS phase [61]. At temperatures low compared to this scale, the proposed lattice plane could then serve as a setting to realize the frustrated J_1-J_2 Kondo lattice and study the anomalous Hall effect.

Note added—Recently, chiral heavy fermion phases and their associated Kondo-destruction transition have also been discussed in the context of moiré structures of transition metal dichalcogenides [62,63].

Acknowledgments—We acknowledge useful discussions with P. Gegenwart, S. Nakatsuji, and P. Goswami. Work at Rice University has primarily been supported by the National Science Foundation under Grant No. DMR-2220603 (W. D. and S. E. G.), by the Air Force Office of Scientific Research under Grant No. FA9550-21-1-0356 (W. D. and S. E. G.), by the Robert A. Welch Foundation Grant No. C-1411 and the Vannevar Bush Faculty Fellowship ONR-VB N00014-23-1-2870 (Q. S.). Work at Anhui University was supported by the National Key R&D Program of the MOST of China under Grant No. 2022YFA1602603 (W. D.). The work in Vienna was supported by the Austrian Science Fund (FWF Grants No. SFB F86 "Q-M&S," I5868-N/FOR5249 "QUAST," and 10.55776/COE1 "quantA") and the European Research Council (ERC Advanced Grant No. 101055088-CorMeTop).

[1] P. Coleman and A. J. Schofield, Nature (London) **433**, 226 (2005).
[2] H. Hu, L. Chen, and Q. Si, arXiv:2210.14183 [Nat. Phys. (to be published)].
[3] S. Kirchner, S. Paschen, Q. Chen, S. Wirth, D. Feng, J. D. Thompson, and Q. Si, Rev. Mod. Phys. **92**, 011002 (2020).
[4] Q. Si, Physica (Amsterdam) **378B**, 23 (2006); Phys. Status Solidi B **247**, 476 (2010).
[5] P. Coleman and A. H. Nevidomskyy, J. Low Temp. Phys. **161**, 182 (2010).
[6] Q. Si, S. Rabello, K. Ingersent, and J. L. Smith, Nature (London) **413**, 804 (2001).
[7] M. S. Kim and M. C. Aronson, Phys. Rev. Lett. **110**, 017201 (2013).
[8] E. D. Mun, S. L. Bud'ko, C. Martin, H. Kim, M. A. Tanatar, J.-H. Park, T. Murphy, G. M. Schmiedeshoff, N. Dilley, R. Prozorov, and P. C. Canfield, Phys. Rev. B **87**, 075120 (2013).
[9] V. Fritsch, N. Bagrets, G. Goll, W. Kittler, M. J. Wolf, K. Grube, C.-L. L. Huang, and H. V. Löhneysen, Phys. Rev. B **89**, 054416 (2014).

[10] Y. Tokiwa, C. Stingl, M.-S. Kim, T. Takabatake, and P. Gegenwart, Sci. Adv. **1**, e1500001 (2015).
[11] S. Nakatsuji, Y. Machida, Y. Maeno, T. Tayama, T. Sakakibara, J. Duijn, L. Balicas, J. Millican, R. T. Macaluso, and J. Y. Chan, Phys. Rev. Lett. **96**, 087204 (2006).
[12] Q. Si and S. Paschen, Phys. Status Solidi B **250**, 425 (2013).
[13] H. Zhao, J. Zhang, M. Lyu, S. Bachus, Y. Tokiwa, P. Gegenwart, S. Zhang, J. Cheng, Y. feng Yang, G. Chen, Y. Isikawa, Q. Si, F. Steglich, and P. Sun, Nat. Phys. **15**, 1261 (2019).
[14] S. Paschen and Q. Si, Nat. Rev. Phys. **3**, 9 (2021).
[15] Y. Machida, S. Nakatsuji, Y. Maeno, T. Tayama, T. Sakakibara, and S. Onoda, Phys. Rev. Lett. **98**, 057203 (2007).
[16] Y. Machida, S. Nakatsuji, S. Onoda, T. Tayama, and T. Sakakibara, Nature (London) **463**, 210 (2010).
[17] G. Chen and M. Hermele, Phys. Rev. B **86**, 235129 (2012).
[18] R. Flint and T. Senthil, Phys. Rev. B **87**, 125147 (2013).
[19] S. B. Lee, A. Paramekanti, and Y. B. Kim, Phys. Rev. Lett. **111**, 196601 (2013).
[20] E.-G. Moon, C. Xu, Y. B. Kim, and L. Balents, Phys. Rev. Lett. **111**, 206401 (2013).
[21] L. Savary, E.-G. Moon, and L. Balents, Phys. Rev. X **4**, 041027 (2014).
[22] M. Udagawa and R. Moessner, Phys. Rev. Lett. **111**, 036602 (2013).
[23] A. Kalitsov, B. Canals, and C. Lacroix, J. Phys. Conf. Ser. **145**, 012020 (2009).
[24] J. G. Rau and H.-Y. Kee, Phys. Rev. B **89**, 075128 (2014).
[25] Y. Tokiwa, J. J. Ishikawa, S. Nakatsuji, and P. Gegenwart, Nat. Mater. **13**, 356 (2014).
[26] S. Paschen, T. Lühmann, S. Wirth, P. Gegenwart, O. Trovarelli, C. Geibel, F. Steglich, P. Coleman, and Q. Si, Nature (London) **432**, 881 (2004).
[27] F. D. M. Haldane, Phys. Rev. Lett. **93**, 206602 (2004).
[28] X. G. Wen, F. Wilczek, and A. Zee, Phys. Rev. B **39**, 11413 (1989).
[29] Y.-C. He, D. N. Sheng, and Y. Chen, Phys. Rev. Lett. **112**, 137202 (2014); S.-S. Gong, W. Zhu, and D. N. Sheng, Sci. Rep. **4**, 6317 (2014).
[30] S. Bieri, L. Messio, B. Bernu, and C. Lhuillier, Phys. Rev. B **92**, 060407(R) (2015).
[31] I. Affleck and J. B. Marston, Phys. Rev. B **37**, 3774 (1988).
[32] See Supplemental Material at http://link.aps.org/supplemental/10.1103/PhysRevLett.133.106504, which includes Refs. [33–37], for a discussion of the six-fermion chiral interactions for both the P_S and P_L phases, the special form of a Hubbard-Stratonovich transformation for the chiral interactions, the Streda and Kubo formulas for the calculation of the Hall conductivity, the reconstruction of the Fermi surfaces and wave functions across the QCP, the saddle-point analysis for the phase diagram, and a proposal for additional materials realization.
[33] S. Florens and A. Georges, Phys. Rev. B **70**, 035114 (2004).
[34] S. Florens and A. Georges, Phys. Rev. B **66**, 165111 (2002).
[35] W. Ding, R. Yu, Q. Si, and E. Abrahams, Phys. Rev. B **100**, 235113 (2019).
[36] K. Sun and E. Fradkin, Phys. Rev. B **78**, 245122 (2008).
[37] M. Oshikawa, Phys. Rev. Lett. **84**, 3370 (2000).
[38] P. Streda, J. Phys. C Solid State Phys. **15**, L717 (1982).
[39] N. Nagaosa, S. Onoda, A. H. MacDonald, and N. P. Ong, Rev. Mod. Phys. **82**, 1539 (2010).
[40] P. Coleman and N. Andrei, J. Phys. Condens. Matter **4057**, 4057 (1989).
[41] F. J. Burnell, S. Chakravarty, and S. L. Sondhi, Phys. Rev. B **79**, 144432 (2009).
[42] N. Sinitsyn, A. MacDonald, T. Jungwirth, V. Dugaev, and J. Sinova, Phys. Rev. B **75**, 045315 (2007).
[43] P. Gegenwart, Q. Si, and F. Steglich, Nat. Phys. **4**, 186 (2008).
[44] T. Ohtsuki, Z. Tian, A. Endo, M. Halim, S. Katsumoto, Y. Kohama, K. Kindo, M. Lippmaa, and S. Nakatsuji, Proc. Natl. Acad. Sci. U.S.A. **116**, 8803 (2019).
[45] P. Chandra, P. Coleman, and R. Flint, Nature (London) **493**, 621 (2013).
[46] B. Ueland, C. Miclea, Y. Kato, O. Ayala-Valenzuela, R. McDonald, R. Okazaki, P. Tobash, M. Torrez, F. Ronning, R. Movshovich, Z. Fisk, E. Bauer, I. Martin, and J. Thompson, Nat. Commun. **3**, 1067 (2012).
[47] M. Kavai, J. Friedman, K. Sherman, M. Gong, I. Giannakis, S. Hajinazar, H. Hu, S. E. Grefe, J. Leshen, Q. Yang, S. Nakatsuji, A. N. Kolmogorov, Q. Si, M. Lawler, and P. Aynajian, Nat. Commun. **12**, 1377 (2021).
[48] H.-H. Lai, S. E. Grefe, S. Paschen, and Q. Si, Proc. Natl. Acad. Sci. U.S.A. **115**, 93 (2017).
[49] L. Chen, C. Setty, H. Hu, M. G. Vergniory, S. E. Grefe, L. Fischer, X. Yan, G. Eguchi, A. Prokofiev, S. Paschen, J. Cano, and Q. Si, Nat. Phys. **18**, 1341 (2022).
[50] S. Dzsaber, L. Prochaska, A. Sidorenko, G. Eguchi, R. Svagera, M. Waas, A. Prokofiev, Q. Si, and S. Paschen, Phys. Rev. Lett. **118**, 246601 (2017).
[51] S. Dzsaber, X. Yan, M. Taupin, G. Eguchi, A. Prokofiev, T. Shiroka, P. Blaha, O. Rubel, S. E. Grefe, H.-H. Lai, Q. Si, and S. Paschen, Proc. Natl. Acad. Sci. U.S.A. **118**, e2013386118 (2021).
[52] L. Chen, F. Xie, S. Sur, H. Hu, S. Paschen, J. Cano, and Q. Si, arXiv:2307.09431.
[53] L. Chen, F. Xie, S. Sur, H. Hu, S. Paschen, J. Cano, and Q. Si, Nat. Commun. **15**, 5242 (2024).
[54] H. Hu and Q. Si, Sci. Adv. **9**, eadg0028 (2023).
[55] H. Shishido, T. Shibauchi, K. Yasu, T. Kato, H. Kontani, T. Terashima, and Y. Matsuda, Science **327**, 980 (2010).
[56] S. K. Goh, Y. Mizukami, H. Shishido, D. Watanabe, S. Yasumoto, M. Shimozawa, M. Yamashita, T. Terashima, Y. Yanase, T. Shibauchi, a. I. Buzdin, and Y. Matsuda, Phys. Rev. Lett. **109**, 157006 (2012).
[57] L. Prochaska, X. Li, D. C. MacFarland, A. M. Andrews, M. Bonta, E. F. Bianco, S. Yazdi, W. Schrenk, H. Detz, A. Limbeck, Q. Si, E. Ringe, G. Strasser, J. Kono, and S. Paschen, Science **367**, 285 (2020).
[58] M. B. Maple and D. Wohlleben, Phys. Rev. Lett. **27**, 511 (1971).
[59] Y. Haga, J. Derr, a. Barla, B. Salce, G. Lapertot, I. Sheikin, K. Matsubayashi, N. K. Sato, and J. Flouquet, Phys. Rev. B **70**, 220406(R) (2004).
[60] P. Wachter, in *Handbook of the Physics and Chemistry of Rare Earths*, edited by K. A. Gschneidner, Jr., L. Eyring,

and S. Hüfner (North-Holland, Amsterdam, 1994), p. 177, Vol. 19.

[61] K. Matsubayashi, K. Imura, H. S. Suzuki, G. Chen, N. Mori, T. Nishioka, K. Deguchi, and N. K. Sato, J. Phys. Soc. Jpn. **76**, 033602 (2007).

[62] A. Kumar, N. C. Hu, A. H. MacDonald, and A. C. Potter, Phys. Rev. B **106**, L041116 (2022).

[63] D. Guerci, J. Wang, J. Zang, J. Cano, J. H. Pixley, and A. Millis, Sci. Adv. **9**, eade7701 (2023).